ChemPubSoc Europe

DOI: 10.1002/slct.201700741

Chemistry SELECT Full Papers

Catalysis

Carbon Nanotube-Modified MnO_2: An Efficient Electrocatalyst for Oxygen Reduction Reaction

Chee Wai Woon,[a] Mohammed Amirul Islam,[a] Baranitharan Ethiraj,[a] Huei Ruey Ong,[a] Chin Kui Cheng,[a, b] Kwok Feng Chong,[c] Gurumurthy Hedge,[d] and Md. Maksudur Rahman Khan*[a, b]

In this work, manganese dioxide/carbon nanotube (MnO_2/CNT) have been synthesized by sonochemical-coprecipitation method and demonstrated that it could be an effective electrocatalyst for oxygen reduction reaction (ORR). Moreover, the effect of CNT inclusion with MnO_2 was also investigated for ORR. The physical and electrochemical properties of the MnO_2/CNT were examined by powder X-ray diffraction (XRD), Fourier Transform Infrared (FT-IR) spectroscopy, Brunauer-Emmett-Teller (BET), Transmission Electron Microscopy (TEM), Field Emission Scanning Electron Microscopy/Energy Dispersive X-ray (FESEM/EDX), Cyclic Voltammetry (CV), Electrochemical Impedance Spectroscopy (EIS), Mott-Schottky and Rotating Disk Electrode (RDE) analysis. CV showed higher currents for the ORR in MnO_2/CNT than CNT; however, ORR current dropped when the MnO_2 loading was increased from 20–40 %. The EIS analysis showed that charge-transfer resistance for MnO_2/CNT was significantly lower compared to the MnO_2 indicating that MnO_2 has good contact with CNT and the composite possess high electrical conductivity. Mott-Schottky results demonstrated that incorporation of CNT into MnO_2 resulted in producing larger electron density in n-type MnO_2/CNT compared to MnO_2 which is liable for efficient electron donation from the Mn^{3+} to adsorbed oxygen in the rate determining step. RDE results showed that MnO_2/CNT follows $4e^-$ transfer pathway, indicating its ability to act as an effective ORR electrocatalyst.

Introduction

Oxygen reduction reaction (ORR) is one of the most extensively studied reactions especially for the application of fuel cell and metal-air batteries.[1] However, ORR is a kinetically slow process which significantly limits the overall reaction kinetics, resulting in a substantial loss in the performance.[2] Therefore, in order to accelerate the reaction, numerous materials have been developed as electrocatalysts.[3] The metals such as platinum (Pt), palladium (Pd), gold (Au) and their alloys exhibit good catalytic activity towards ORR.[4] Among them, Platinum (Pt) is the most commonly used electrocatalyst for the ORR due to its higher electrocatalytic activity and stability.[5] But, though the Pt has good catalytic activity, the high cost along with the catalyst poisoning limits its practical applications.[6] So, several cheap alternative materials have been used as electrocatalysts to increase the ORR.[1a] Among them, non-precious metals such as manganese oxides had been widely investigated as one of the most promising catalysts for ORR[7] both in fuel cells and in metal-air batteries applications due to its distinctive properties such as lower cost, easier preparation, good ORR catalytic activity and least harmful to the environment.[8] Stoerzinger, et al.[9] reported that among the catalysts, manganese based oxides have the highest activities close to that of precious metals. The same group also reported that α-MnO_2 possesses higher activity per cost (approximated on a metal basis) than Pt/C.

Besides that, in ORR, the 4-electron reduction reaction is favourable since the 2-electron reduction reaction could involve in hydrogen peroxide production leading to high over potential.[8b,10] However, the poor electrical conductivity restricts the electrochemical activity of manganese oxides. Therefore, several kinds of materials such as Graphite, Monarch carbon black 1000 and Vulcan XC-72 have been used as conductive supports to increase the ORR performance.[11] However, these materials have poor ORR activity.[12] So, in order to enhance the ORR performance of MnO_2, a better electron conducting material can be incorporated, such as multiwalled carbon nanotubes (MWCNTs), which possess excellent electronic conductivity, high thermal stability, chemical stability, high porosity, high surface area, nano-size morphology and good mechanical

[a] C. W. Woon, M. A. Islam, Dr. B. Ethiraj, Dr. H. R. Ong, Prof. Dr. C. K. Cheng, Prof. Dr. Md. M. R. Khan
Faculty of Chemical and Natural Resources Engineering
Universiti Malaysia Pahang
26300 Gambang Pahang, Malaysia
E-mail: mrkhancep@yahoo.com
[b] Prof. Dr. C. K. Cheng, Prof. Dr. Md. M. R. Khan
Centre of Excellence for Advanced Research in Fluid Flow
Universiti Malaysia Pahang
26300 Gambang Pahang, Malaysia
[c] Prof. Dr. K. F. Chong
Faculty of Industrial Sciences & Technology
Universiti Malaysia Pahang
26300 Gambang Pahang, Malaysia
[d] Prof. Dr. G. Hedge
Centre for Nano-Materials & Displays
BMS College of Engineering
Basavanagudi, 560019 Bangalore, India

Supporting information for this article is available on the WWW under https://doi.org/10.1002/slct.201700741

properties.[13] Thus, the incorporation of MnO_2 into the CNT can develop an efficient ORR electrocatalyst which could potentially replace the precious-metal electrocatalysts such as Pt and gold. Khilari, et al.[11] reported that the MnO_2-NTs/graphene composite with fixed loading showed a higher ORR activity than the MnO_2-NTs/Vulcan XC and MnO_2-NTs/MWCNTs composites but the effect of CNT inclusion with MnO_2 and their mechanisms have never been studied. Therefore, the present study is intended to elucidate the effect of CNT inclusion with MnO_2 for ORR and identify their mechanism using RDE (Rotating disk electrode) experiments and Mott-Schottky analysis.

Results and Discussion

XRD analysis of MnO_2/CNT

The phase and crystalline nature of the as-prepared MnO_2/CNT was studied using XRD and presented in Figure 1. The peaks at

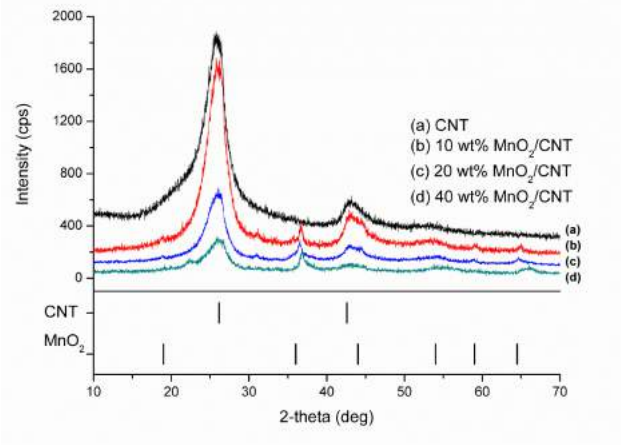

Figure 1. XRD patterns of CNT (a), 10% (b), 20% (c) and 40% (d) of MnO_2/CNT.

2θ of 26.14° and 42.60° correspond to the (0 0 2) and (1 0 0) plane of carbon, respectively which is in agreement with Liew, et al.,[8a] Safari and Gandomi-Ravandi,[14a] Zhao, et al.[14b] Other intense peaks were found at 2θ of 19°, 36°, 44°, 54°, 59° and 64.5° which can be indexed as (2 0 0), (2 1 1), (3 0 1), (6 0 0), (5 2 1) and (0 0 2), respectively. These peaks can be ascribed to the characteristic peaks of MnO_2.[8d,13a,15] The average crystallite size of the MnO_2 in the as-prepared electrocatalyst was calculated based on the MnO_2 (2 1 1) peaks by using Scherrer's equation, $t=(0.9\lambda)/(\beta\cos\theta)$ where t is the grain size, λ is the wavelength of the radiation used and β is an angular width. The average crystallite size of the MnO_2 was determined to be 9.74 nm.

FT-IR analysis of MnO_2/CNT

The formation of MnO_2/CNT is further investigated with FT-IR Spectroscopy and presented in Figure 2. The correlative assign-

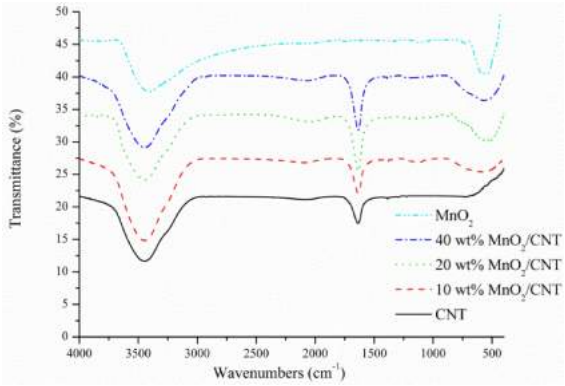

Figure 2. FT-IR spectra of CNT, MnO_2, 10 wt%, 20 wt% and 40 wt% of MnO_2/CNT.

Table 1. FT-IR Band Assignments of CNT, MnO_2, 10 wt%, 20 wt% and 40 wt% of MnO_2/CNT

Catalyst	Observed frequencies (cm^{-1})	Band assignments	Reference
CNT	3447	OH (stretch)	[16]
	1654	C=O (stretch)	[14a,16b]
MnO_2	3442	OH (stretch)	[16]
	562	Mn–O and Mn–O-Mn	[16b]
10 wt%	3446	OH (stretch)	[16]
	1653	C=O (stretch)	[14a,16b]
	1110	C–O (stretch)	[17]
	567	Mn–O and Mn–O-Mn	[16b]
20 wt%	3446	OH (stretch)	[16]
	1655	C=O (stretch)	[14a,16b]
	1115	C–O (stretch)	[17]
	544	Mn–O and Mn–O-Mn	[16b]
40 wt%	3443	OH (stretch)	[16]
	1654	C=O (stretch)	[14a,16b]
	1118	C–O (stretch)	[17]
	544	Mn–O and Mn–O-Mn	[16b]

ments of the FTIR peaks are presented in Table 1. The broad band observed at 3440–3500 cm^{-1} can be ascribed to the bending vibrations of adsorbed molecular water and stretching vibrations of OH groups.[16] The peaks at ca. 1654 cm^{-1} can be attributed to C=O stretching vibration of the samples except for the MnO_2 which is in agreement with Safari and Gandomi-Ravandi,[14a] Xie and Gao.[16b] In addition, around 1110 cm^{-1}, a very weak peak was observed in all the MnO_2/CNT samples

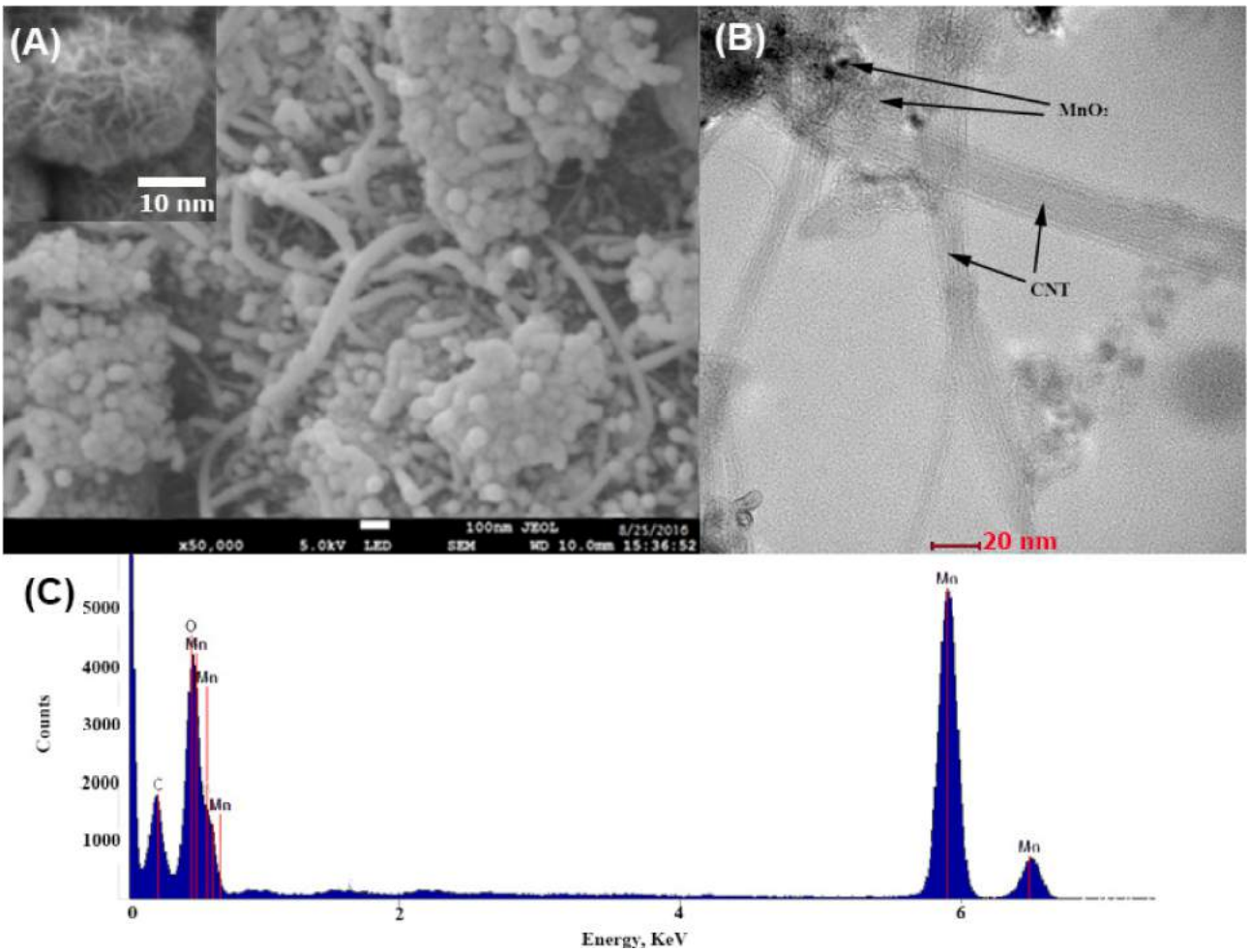

Figure 3. Morphology and elemental analysis of 20 wt% MnO_2/CNT by (a) FESEM (inset: Magnification of 200k), (b) TEM and (c) EDX.

except in CNT and MnO_2, which corresponds to C–O stretching vibrations of the samples.[17] At the low frequency region, sharp peaks were found in all the MnO_2/CNT samples except CNT. Those peaks are attributed to the Mn–O and Mn-O–Mn vibrations in [MnO_6] octahedral.[16b]

The morphology and elemental analysis of the as-prepared MnO_2/CNT was examined by FESEM/EDX and TEM as demonstrated in Figure 3. From the FESEM image (Figure 3a), it can be seen that, the CNT was roughened by the formation of crystal structures of MnO_2. The nano-sized structure of MnO_2/CNT was then visualized under TEM (Figure 3b). It can be observed that the particle size of MnO_2 crystals is about 10–20 nm. Besides that, the EDX analysis shown in Figure 3c confirmed the presence of C, O and Mn, which indicated that the high purity of MnO_2/CNT was synthesized and the results are in consistent with the XRD results (Figure 1).

BET analysis of MnO_2/CNT

The specific surface area of the as-prepared MnO_2/CNT was investigated by using BET analysis. As shown in Table 2, the measured BET specific surface areas are 348.11, 81.12, 351.36, 318.18 and 283.24 m^2/g for CNT, MnO_2, 10 wt%, 20 wt% and 40 wt% of MnO_2/CNT respectively. The increase of MnO_2 loading onto the CNT resulted in a decrease in BET surface area. Bezerra, et al.,[18a] Sun, et al.[18b] reported that the surface area reduced linearly with an increase in metal loading which might due to the blockage of pores in the support by metal particles, or the metal chelate or else its fragments that could chemically bond onto the support surface.

Table 2. BET Surface Area of MnO_2/CNT

Catalyst	BET surface area (m^2/g)
CNT	348.11
MnO_2	81.12
10 wt% MnO_2/CNT	351.36
20 wt% MnO_2/CNT	318.18
40 wt% MnO_2/CNT	283.24

ORR activity of MnO_2/CNT

The ORR activity of different compositions of MnO_2/CNT was evaluated and compared with CNT by using Cyclic Voltammetry

(CV) and presented in Figure 4. It can be seen that the ORR peaks of the MnO_2 catalysts on CNTs are in between −0.2 and

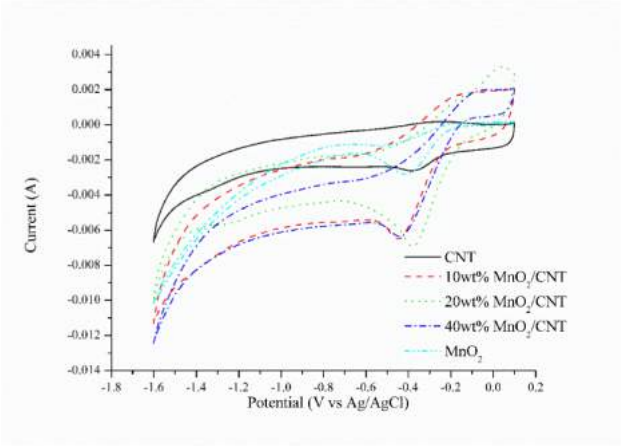

Figure 4. CV of CNT, MnO_2, 10 wt%, 20 wt% and 40 wt% of MnO_2/CNT for ORR in 0.1 M of the oxygenated Na_2SO_4 aqueous solution in the potential range from −1.6 to +0.1 V at the scan rate of 30 mV/s.

−0.4 V as reported by Zhang, et al.,[8d] Lu, et al.,[15b] Lu, et al.[19] CNT was used as a control in the experiment, and only a small ORR peak appeared which might due to the CNT defects.[8a,15b,20] The doping of MnO_2 onto CNT has increased the ORR current about 2.5 times than that of CNT which demonstrates that the MnO_2/CNT has higher ORR catalytic activity than CNT. The increase of ORR catalytic activity might be due to the mutualistic interaction between the MnO_2 and carbon support CNT because it could have increased the electrical conductivity and thereby enhanced the catalytic activity of MnO_2/CNT.[21] The active carbon support can offer a large surface for the deposition and well dispersion of MnO_2. In addition, the enhanced surface area of MnO_2/CNT electrocatalysts helped to increase the number of active sites which in turn improved the contact between catalyst and electrolyte material.[21] Among the compositions of MnO_2/CNT, 20 wt% of MnO_2/CNT showed highest ORR current and potential (-0.0069 A, −0.38 V) compared to 10 wt% (-0.0065 A, −0.45 V) and 40 wt% (-0.0064 A, −0.44 V) of MnO_2/CNT. These results clearly showed that the optimum loading of MnO_2 onto CNT is 20 wt%.

Electrochemical impedance spectroscopy of MnO_2/CNT

The electrochemical properties of the as-prepared MnO_2/CNT were examined using Electrochemical Impedance Spectroscopy (EIS) and presented in Figure 5b. The EIS data were calculated by fitting the EIS spectra to a simple Randles circuit (Figure 5a) and shown in Table 3. The Randles circuit consists of solution resistance (R_s), constant phase element (CPE), charge-transfer resistance (R_{ct}) and the Warburg impedance (W_o). CPE was used to replace the capacitor in the Randles circuit in order to compensate the non-homogeneity in the system. The capacitance (C) can be estimated by using Eq. 1.

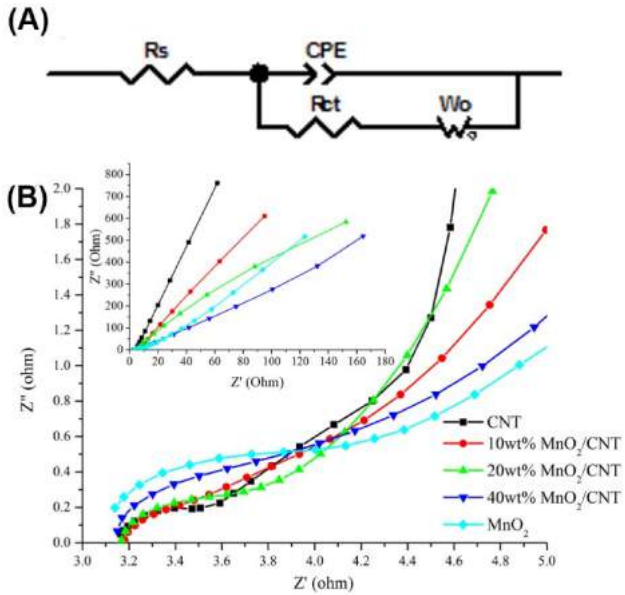

Figure 5. (a) Randles circuit (b) Nyquist plots of EIS by CNT, MnO_2, 10 wt%, 20 wt% and 40 wt% of MnO_2/CNT; Full range of Nyquist plot is shown in the inset.

Table 3. Electrochemical Parameters Obtained by Fitting EIS Data.

Elements	CNT	MnO_2	10 wt%	20 wt%	40 wt%
R_s (Ω)	3.14	2.92	3.16	3.13	3.10
C (F)	1.31 x10^{-4}	5.78 x10^{-5}	1.64 x10^{-4}	1.51 x10^{-4}	4.81 x10^{-5}
R_{ct} (Ω)	0.56	2.07	0.73	0.97	1.47
W_R (Ω)	3.51	7.00	5.34	3.52	5.91
W_T	5.64 x10^{-2}	5.69 x10^{-2}	7.73 x10^{-2}	3.40 x10^{-2}	2.11 x10^{-2}
W_P	0.48	0.37	0.44	0.45	0.38
R_{total} (Ω)	7.21	11.98	9.23	7.62	10.48

$$C = R^{1-n/n}Q^{1/n} \quad (1)$$

where C, R, n and Q are the capacitance, parallel resistance, empirical constant and pseudo-capacitance, respectively.[22]

W_o represents the process of diffusion of ions from the electrolyte to the interface and which has three parts: ohmic resistance (W_R), capacitive part (W_T) and its exponent (W_P) while total resistance (R_{total}) is the sum of all the individual (R_s, R_{ct} and W_R) resistances.[23] From Table 3, it can be seen that the R_s of the all the as-prepared catalysts were almost similar. Whereas the charge-transfer resistance of MnO_2 is higher (2.07 Ω) but with the increase in the concentration of CNT (40 wt%, 20 wt%, 10 wt% and 0 wt% of MnO_2) the charge transfer resistance of MnO_2/CNT (1.47, 0.97, 0.73 and 0.56) decreased as shown in Figure 5b. Similar results were also reported by other literatures where CNT exhibited the lowest R_{ct} but increased proportionally with the increase in MnO_2 loading.[16b,24] The higher R_{ct} of MnO_2 was due to the poor electrical conductivity and with the increase in CNT concentration, the R_{ct} decreased.[24a] Therefore, the increase in the loading of MnO_2 in MnO_2/CNT nanocomposite increases the Rct. The results also demonstrated

that 20 wt% MnO_2/CNT has the lowest W_R (3.52 Ω) among the MnO_2/CNT compositions but it is slightly higher than CNT (3.51 Ω).

The Mott-Schottky plot of MnO_2 and MnO_2/CNT is shown in Figure 6. From the Mott-Schottky equation, a linear relationship of $1/C^2$ versus applied potential can be obtained (Eq. 2).[1a]

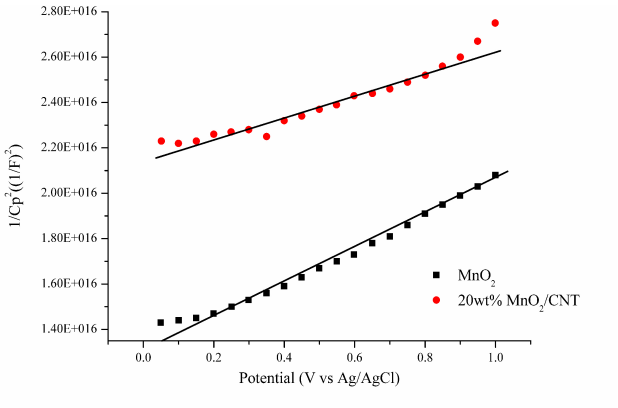

Figure 6. Mott-Schottky plots of MnO_2 and 20 wt% MnO_2/CNT.

$$(1/C_{SC})^2 = 2/e\varepsilon\varepsilon_o N_D(E - E_{fb} - KT/e) \quad (2)$$

where C_{SC} is space-charge capacities, ε_o is permittivity of free space, e is the charge of the electron, ε is a dielectric constant of MnO_2/CNT, E_{fb} is flat-band potential, E is applied potential, k is Boltzmann constant, N_D is donor density and T is Kelvin temperature. The negative and positive slopes correspond to p- and n-type conductivities, respectively.[25] It can be seen from the Figure 6 that the Mott-Schottky plots of MnO_2/CNT have positive slopes which indicate the presence of n-type semiconductors. The flat band potential (E_{fb}) can be approximately calculated by extrapolating the linear Mott-Schottky plot (Figure 6). The E_{fb} values of the electrocatalysts were −1.43 V and −4 V for MnO_2 and MnO_2/CNT respectively. From the slope of the linear part of the plot close to the flat-band potential $2/(e\varepsilon\varepsilon_D N_D)$, shows that the slope of MnO_2/CNT is smaller than MnO_2. The incorporation of MnO_2 onto the CNT reduced the slope, which implies that the charge carrier density is larger for MnO_2/CNT than that of MnO_2. Similar results were reported by Basirun, et al.[1a] Therefore, the incorporation of MnO_2 onto CNT can result in rapid electron donation, and that in turn increases the pace of the rate determining step of the oxygen reduction reaction. The Mott-Schottky results showed that the incorporation of CNT into MnO_2 resulted in producing larger electron density in MnO_2/CNT composite than the MnO_2 which is liable for the efficient electron donation from the Mn^{3+} to adsorbed oxygen in the rate determining step leading to higher ORR activity.

Rotating disk electrode experiments

The as-prepared MnO_2 and 20 wt% MnO_2/CNT were coated on the RDE for electrochemical experiments.[26] The LSVs of ORR that were recorded on RDEs for MnO_2 and 20 wt% MnO_2/CNT are shown in Figure 7a and b, respectively. It can be seen that the onset potential and half wave potential of ORR on MnO_2/CNT are −0.01 V and −0.2 V, respectively which are more positive than that of MnO_2, indicating the importance of CNT injunction.[27] The limiting current densities of MnO_2 and MnO_2/CNT were increased from 0.54 to 0.75 mA/cm^2 and 2.01 to 3.85 mA/cm^2, respectively when rotation rates were increased from 400 to 3600 rpm. Higher rotational rates cause rapid oxygen flux to the surface of the electrode and thereby obtained large currents.

The Koutecky-Levich (K–L) plot was constructed from rotation speed-dependent current-potential data according to the Eq.3 to examine the ORR kinetics.[26]

$$\frac{1}{i} = \frac{1}{i_k} + \frac{1}{i_d} = -\frac{1}{nFAkC^0} - \frac{1}{0.62nFAD_{O_2}^{\frac{2}{3}} v^{-\frac{1}{6}} C^0 \omega^{\frac{1}{2}}} \quad (3)$$

where i is the measured current, i_k is the kinetic current, i_d is the diffusion-limiting current, F is Faraday constant, n is the overall number of electron transferred, A is the geometric electrode area (cm^2), k is the rate constant for oxygen reduction, C^0 is the saturated concentration of oxygen in 0.1 M potassium hydroxide (1.14×10^{-6} mol/cm^3), D_{O2} is the diffusion coefficient of oxygen (1.73×10^{-5} cm^2/s), w is the rotation rate (rad/s) and v is the kinetic viscosity of solution (0.01 cm^2/s).

The number of electrons (n) participated in the oxygen reduction reaction is a key factor for assessing the catalyst performance.[28] The slopes of the K–L curves were used to calculate the n value on the basis of the Koutecky-Levich equation (Eq. 3). Figure 7c and d demonstrates the Koutecky-Levich plots at various electrode potentials for the MnO_2 and 20 wt% MnO_2/CNT, respectively. The n value during ORR was determined to be 2.19 and 3.91 for MnO_2 and 20 wt% MnO_2/CNT, respectively.

Based on the RDE results, it is implied that the MnO_2 and MnO_2/CNT followed 2e and 4e mechanism, respectively because their apparent n values are 2.19 and 3.91 which are close to the theoretical values for 2e and 4e$^-$ reduction of O_2, respectively. Dumitru, et al.[29] reported that after the acid modification of CNT, the number of C–O functional groups was increased on the surface of the CNTs, which, in turn, increased the electrocatalytic activity, leading to 4e- pathway for the ORR. Whereas, in this study, during the preparation of MnO_2/CNT, highly oxidizing agents such as $KMnO_4$ and H_2SO_4 were used which might have oxidized the CNTs as it can be observed from the very weak peak (at 1110 cm^{-1}) of C–O group in the FTIR of MnO_2/CNT (Figure. 2). Thus, it is assumed that the presence of C–O groups in the MnO_2/CNT shifted the ORR from 2 electron pathway to 4 electron pathway. Moreover, the morphology of the electrocatalyst also plays a crucial role in influencing the electron transfer pathway. Recently, Selvakumar, et al.[7a] re-

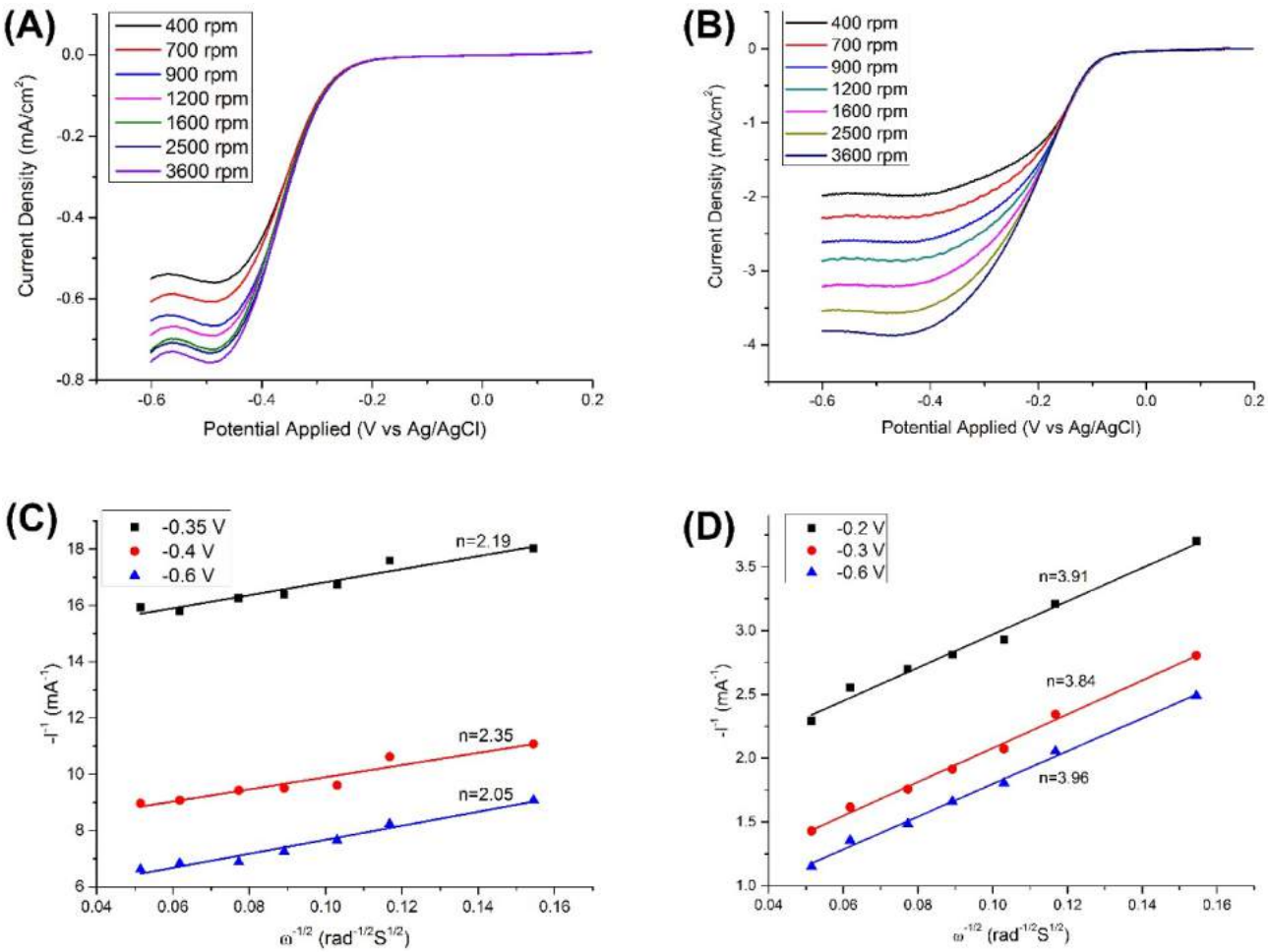

Figure 7. LSV curves of (a) MnO_2 and (b) 20 wt% MnO_2/CNT obtained from RDE measurements at various rotating rates from 400 rpm to 1600 rpm at a scan rate of 10 mV s^{-1} in oxygen saturated 0.1 M KOH solution; K–L plots of ORR for the samples of (c) MnO_2 and (d) 20 wt% MnO_2/CNT.

ported that nanoshapes of MnO_2 influence the electron transfer pathway. So, it is assumed that MnO_2/CNT nanostructure might have favoured the 4 electron transfer pathway. This feature can be better visualized by remembering that the mechanism followed by the ORR relies on the kind of interaction between the catalyst surface and the oxygen molecules. It is known that the O_2 molecules adsorb in a horizontal mode on manganese oxide surfaces proceed through a bridge-type configuration.[12] Bridge-type interactions conduct to the dissociation of O_2, which is consistent with the $4e^-$ reduction pathway. In contrast, ORR follows 2e- reduction pathway if the interaction between catalyst surface and O_2 molecules are in the vertical or end-on mode of adsorption.[7a] So, the incorporation of CNT into MnO_2 might have provided the optimum requirement for the adsorbed oxygen in a bridge mode which would have favoured the $4e^-$ reduction pathway whereas MnO_2 might have formed the end-on mode of adsorption and led to 2e- reduction pathway.

Besides that, Gong, et al.[30] proved that, CNT possess poor electrocatalytic activity. Therefore, the main electrocatalytic activity was contributed by MnO_2, while CNT functioned as support for MnO_2, to provide better electrical conductivity and 3D matrix for the composite structure. Xu, et al.[31] reported that majority of the metal oxides generally have poor electrical conductivity compared with carbon-based materials, which could limit the transfer of an electron to their catalytically active sites. So, doping of metal oxides with nano carbons can help to form the conducting network, which facilitates the charge transfer during the electrochemical reactions at the oxide surfaces. In addition, Zhang, et al.,[32a] Fu, et al.[32b] reported that the integration of metal oxide and nano-structural carbon such as graphene and CNT to produce electrocatalysts for ORR could have enhanced both the electrocatalytic activity and stability. This might be due to their large surface area, high conductivity and high electrochemical stability.[27] Moreover, based on our BET results, it can be observed that the surface area of 20 wt% MnO_2/CNT is 4 times higher than MnO_2. Therefore, 20 wt% MnO_2/CNT can allow more active sites and that can improve the contact between catalyst and electrolyte.[33] Furthermore, the electrical conductivity of the MnO_2/CNT is better than MnO_2 as evidenced by EIS data where R_{ct} of MnO_2 is higher than MnO_2/CNT. Apart from that, Mott-Schottky results revealed that

MnO_2/CNT possesses higher electron density than MnO_2, as the slope of MnO_2/CNT is smaller than MnO_2. The increased electron density enhanced the conductivity and facilitated the charge separation,[34] which is responsible for the efficient electron donation from Mn to adsorbed oxygen in the rate determining step leading to higher ORR activity. Cheng, et al.[33] also mentioned that electrical conductivity plays a key role in influencing the catalytic activity. Moreover, it is important to note from the CV data that the 20 wt% MnO_2/CNT exhibited highest ORR current (-0.0069 A) than MnO_2 (-0.0028 A). Furthermore, the onset potential and half-wave potential for ORR on MnO_2/CNT catalyst are found to be −0.01 V and −0.2 V, respectively, which are more positive than that of MnO_2. On the basis of the onset potentials, half-wave potentials and CV, one can conclude that MnO_2/CNT catalyst is much more active than MnO_2 for the ORR.

Conclusions

MnO_2/CNT nanoparticles were successfully prepared using sonochemical-coprecipitation method. The FESEM/EDX, TEM, XRD, BET and FT-IR revealed the morphological crystalline structures and elemental analysis of nanostructured as-prepared MnO_2/CNT. The CV results showed that the ORR activity of MnO_2/CNT is 2.5 times higher than CNT. Among the compositions of MnO_2/CNT, 20 wt% of MnO_2/CNT showed the optimum catalyst loading that generated the highest ORR current (-0.0069 A) with the lowest total (R_{total}) resistance (7.62 Ω). Moreover, from the Mott-Scottky analysis, it is clear that the incorporation of CNT into MnO_2 can produce larger electron density in n-type MnO_2/CNT compared to the MnO_2 which is liable for efficient electron donation from the Mn^{3+} to adsorbed oxygen in the rate determining step leading to higher ORR activity. Furthermore, RDE investigations revealed that MnO_2/CNT and MnO_2 follow the quasi-4 electron transfer and 2 electron transfer pathways, respectively. Thus, MnO_2/CNT proved to be an efficient electrocatalyst for the ORR compared to the MnO_2 catalyst.

Acknowledgements

This work was financially supported by the research grant (Project No: RDU 140322; GRS 150321) from Universiti Malaysia Pahang, Malaysia.

Conflict of Interest

The authors declare no conflict of interest.

Keywords: Catalyst · Electrochemical properties · MnO_2/CNT · Oxygen reduction reaction

[1] a) W. J. Basirun, M. Sookhakian, S. Baradaran, Z. Endut, M. R. Mahmoudian, M. Ebadi, R. Yousefi, H. Ghadimi, S. Ahmed, *Sci. Report.* **2015**, *5*, 9108; b) H. A. Gasteiger, N. M. Marković, *Science* **2009**, *324*, 48–49; c) G. Wu, P. Zelenay, *Acc. Chem. Res.* **2013**, *46*, 1878–1889.

[2] K. Lee, L. Zhang, H. Lui, R. Hui, Z. Shi, J. Zhang, *Electrochim. Acta* **2009**, *54*, 4704–4711.

[3] a) S. Pandit, A. Sengupta, S. Kale, D. Das, *Bioresour. Technol.* **2011**, *102*, 2736–2744; b) M. A. Rodrigo, P. Cañizares, J. Lobato, *Bioresour. Technol.* **2010**, *101*, 7014–7018.

[4] a) M. K. Carpenter, T. E. Moylan, R. S. Kukreja, M. H. Atwan, M. M. Tessema, *J. Am. Chem. Soc.* **2012**, *134*, 8535–8542; b) C. Koenigsmann, E. Sutter, R. R. Adzic, S. S. Wong, *J. Phys. Chem. C* **2012**, *116*, 15297–15306.

[5] a) C. Song, J. Zhang, in *PEM fuel cell electrocatalysts and catalyst layers*, Springer, **2008**, pp. 89–134; b) B. C. Steele, A. Heinzel, *Nature* **2001**, *414*, 345–352; c) C. W. Woon, H. R. Ong, K. F. Chong, K. M. Chan, M. M. R. Khan, *Procedia Chem.* **2015**, *16*, 640–647.

[6] a) H. Dong, H. Yu, X. Wang, *Environ. Sci. Technol.* **2012**, *46*, 13009–13015; b) L. Wang, P. Liang, J. Zhang, X. Huang, *Bioresour. Technol.* **2011**, *102*, 5093–5097; c) Z. Yang, H. Nie, X. a. Chen, X. Chen, S. Huang, *J. Power Sources* **2013**, *236*, 238–249.

[7] a) K. Selvakumar, S. M. Senthil Kumar, R. Thangamuthu, K. Ganesan, P. Murugan, P. Rajput, S. N. Jha, D. Bhattacharyya, *J. Phys. Chem. C* **2015**, *119*, 6604–6618; b) Q. Yu, J. Xu, C. Wu, J. Zhang, L. Guan, *ACS Appl. Mater. Interfaces* **2016**; c) L. Li, X. Feng, Y. Nie, S. Chen, F. Shi, K. Xiong, W. Ding, X. Qi, J. Hu, Z. Wei, *ACS Catal.* **2015**, *5*, 4825–4832; d) A. R. Mainar, L. C. Colmenares, O. Leonet, F. Alcaide, J. J. Iruin, S. Weinberger, V. Hacker, E. Iruin, I. Urdanpilleta, J. A. Blazquez, *Electrochim. Acta* **2016**, *217*, 80–91; e) A. Flegler, S. Hartmann, H. Weinrich, M. Kapuschinski, J. Settelein, H. Lorrmann, G. Sextl, *C* **2016**, *2*, 4; f) I. M. Mosa, S. Biswas, A. M. El-Sawy, V. Botu, C. Guild, W. Song, R. Ramprasad, J. F. Rusling, S. L. Suib, *J. Mater. Chem. A* **2016**, *4*, 620–631.

[8] a) K. B. Liew, W. R. W. Daud, M. Ghasemi, K. S. Loh, M. Ismail, S. S. Lim, J. X. Leong, *Int. J. Hydrogen Energy* **2015**, *40*, 11625–11632; b) X.-W. Liu, X.-F. Sun, Y.-X. Huang, G.-P. Sheng, K. Zhou, R. J. Zeng, F. Dong, S.-G. Wang, A.-W. Xu, Z.-H. Tong, *Water Res.* **2010**, *44*, 5298–5305; c) F. H. Lima, M. L. Calegaro, E. A. Ticianelli, *J. Electroanal. Chem.* **2006**, *590*, 152–160; d) L. Zhang, C. Liu, L. Zhuang, W. Li, S. Zhou, J. Zhang, *Biosens. Bioelectron.* **2009**, *24*, 2825–2829.

[9] K. A. Stoerzinger, M. Risch, B. Han, Y. Shao-Horn, *ACS Catal.* **2015**, *5*, 6021–6031.

[10] a) M. Chatenet, M. Aurousseau, R. Durand, F. Andolfatto, *J. Electrochem. Soc.* **2003**, *150*, D47-D55; b) K. B. Liew, W. R. W. Daud, M. Ghasemi, J. X. Leong, S. S. Lim, M. Ismail, *Int. J. Hydrogen Energy* **2014**, *39*, 4870–4883.

[11] S. Khilari, S. Pandit, D. Das, D. Pradhan, *Biosens. Bioelectron.* **2014**, *54*, 534–540.

[12] I. Roche, E. Chaînet, M. Chatenet, J. Vondrák, *J. Phys. Chem. C* **2007**, *111*, 1434–1443.

[13] a) Y. Zhang, Y. Hu, S. Li, J. Sun, B. Hou, *J. Power Sources* **2011**, *196*, 9284–9289; b) C. Wang, D. Li, C. O. Too, G. G. Wallace, *Chem. Mater.* **2009**, *21*, 2604–2606; c) D. A. Brownson, D. K. Kampouris, C. E. Banks, *J. Power Sources* **2011**, *196*, 4873–4885.

[14] a) J. Safari, S. Gandomi-Ravandi, *J. Mol. Catal. A: Chem.* **2013**, *373*, 72–77; b) Y. Zhao, R. Nakamura, K. Kamiya, S. Nakanishi, K. Hashimoto, *Nat. Commun.* **2013**, *4*.

[15] a) S. Liang, F. Teng, G. Bulgan, R. Zong, Y. Zhu, *J. Phys. Chem. C* **2008**, *112*, 5307–5315; b) M. Lu, S. Kharkwal, H. Y. Ng, S. F. Y. Li, *Biosens. Bioelectron.* **2011**, *26*, 4728–4732; c) V. Subramanian, H. Zhu, B. Wei, *J. Power Sources* **2006**, *159*, 361–364.

[16] a) V. Gupta, T. A. Saleh, *Syntheses of carbon nanotube-metal oxides composites; adsorption and photo-degradation*, INTECH Open Access Publisher Rijeka, Croatia, **2011**; b) X. Xie, L. Gao, *Carbon* **2007**, *45*, 2365–2373.

[17] a) M. A. Salam, *Arabian J. Chem.* **2012**, *5*, 291–296; b) S. Sankal, C. Kaynak, *J. Reinf. Plast. Compos.* **2013**, *32*, 75–86.

[18] a) C. W. Bezerra, L. Zhang, K. Lee, H. Liu, A. L. Marques, E. P. Marques, H. Wang, J. Zhang, *Electrochim. Acta* **2008**, *53*, 4937–4951; b) G.-Q. Sun, J.-T. Wang, S. Gupta, R. Savinell, *J. Appl. Electrochem.* **2001**, *31*, 1025–1031.

[19] M. Lu, L. Guo, S. Kharkwal, H. Y. Ng, S. F. Y. Li, *J. Power Sources* **2013**, *221*, 381–386.

[20] D. Ye, T. Wu, H. Cao, Y. Wang, B. Liu, S. Zhang, J. Kong, *RSC Adv.* **2015**, *5*, 26710–26715.

[21] G. G. Kumar, Z. Awan, K. S. Nahm, J. S. Xavier, *Biosens. Bioelectron.* **2014**, *53*, 528–534.

[22] C. M. Gore, J. O. White, E. D. Wachsman, V. Thangadurai, *J. Mater. Chem. A* **2014**, *2*, 2363–2373.

[23] a) Z. Jovanovic, G.-o. BuicĂ, V. Miskovic-Stankovic, E.-M. Ungureanu, C.-A. Amarandei, *UPB Scientific Bulletin, Series B: Chemistry and Materials Science* **2013**, *75*, 125–134; b) A. Ter Heijne, O. Schaetzle, S. Gimenez, F. Fabregat-Santiago, J. Bisquert, D. P. Strik, F. Barriere, C. J. Buisman, H. V. Hamelers, *Energy Environ. Sci.* **2011**, *4*, 5035–5043.
[24] a) W.-Y. Ko, Y.-F. Chen, K.-M. Lu, K.-J. Lin, *Sci. Rep.* **2016**, *6*; b) H. Wang, C. Peng, F. Peng, H. Yu, J. Yang, *Mater. Sci. Eng. B* **2011**, *176*, 1073–1078; c) H. Xia, Y. Wang, J. Lin, L. Lu, *Nanoscale Res. Lett.* **2012**, *7*, 1.
[25] H. Wang, Y. Liu, M. Li, H. Huang, H. Xu, R. Hong, H. Shen, *Optoelectron. Adv. Mater. Rapid Commun* **2010**, *4*, 1166–1169.
[26] A. J. Bard, L. R. Faulkner, *Electrochemical methods: fundamentals and applications, Vol. 2*, Wiley New York, **2000**.
[27] N. Xu, Y. Liu, X. Zhang, X. Li, A. Li, J. Qiao, J. Zhang, *Sci. Report.* **2016**, *6*.
[28] W. Xiao, D. Wang, X. W. Lou, *J. Phys. Chem. C* **2009**, *114*, 1694–1700.
[29] A. Dumitru, M. Mamlouk, K. Scott, *Electrochim. Acta* **2014**, *135*, 428–438.
[30] K. Gong, P. Yu, L. Su, S. Xiong, L. Mao, *J. Phys. Chem. C* **2007**, *111*, 1882–1887.
[31] N. Xu, J. Qiao, X. Zhang, C. Ma, S. Jian, Y. Liu, P. Pei, *Appl. Energy* **2016**, *175*, 495–504.
[32] a) B. Zhang, Z. Wen, S. Ci, S. Mao, J. Chen, Z. He, *ACS Appl. Mater. Interfaces* **2014**, *6*, 7464–7470; b) X. Fu, J. Jin, Y. Liu, Z. Wei, F. Pan, J. Zhang, *ACS Appl. Mater. Interfaces* **2014**, *6*, 3930–3936.
[33] F. Cheng, Y. Su, J. Liang, Z. Tao, J. Chen, *Chem. Mater.* **2009**, *22*, 898–905.
[34] X. Zhao, J. Feng, S. Chen, Y. Huang, T. C. Sum, Z. Chen, *Phys. Chem. Chem. Phys.* **2017**, *19*, 1074–1082.

Submitted: April 7, 2017
Revised: August 20, 2017
Accepted: August 24, 2017